Journal of the Mechanics and Physics of Solids 61 (2013) 161–174

Contents lists available at SciVerse ScienceDirect

Journal of the Mechanics and Physics of Solids

journal homepage: www.elsevier.com/locate/jmps

The mechanical behavior of porous metal fiber sintered sheets

M.Z. Jin [a,b], C.Q. Chen [a,*], T.J. Lu [c]

[a] Department of Engineering Mechanics, CNMM & AML, Tsinghua University, Beijing 100084, China
[b] Department of Mechanical Engineering, University of Alberta, Edmonton, Canada T6G2G8
[c] State Key Laboratory for Mechanical Structure Strength and Vibration, Xi'an Jiaotong University, Xi'an 710049, China

ARTICLE INFO

Article history:
Received 14 January 2012
Received in revised form
25 June 2012
Accepted 14 August 2012
Available online 27 August 2012

Keywords:
Porous metal fiber sintered sheets
Foam material
Elastic-plastic material
Constitutive behavior
Finite element

ABSTRACT

Porous metal fiber sintered sheets (MFSSs) are a type of low density cellular materials promising for functional and structural applications. A micromechanics random beam model is proposed to investigate the elasto-plastic behavior of MFSSs. The relative density dependence of the elastic constants and yield strength of MFSSs is predicted and found to agree well with available experimental results. Fiber stretching is identified as the dominant deformation mechanism under uniaxial and multiaxial loading. When compared with two-dimensional Voronoi foams and honeycombs, the stretching deformation dominated MFSSs exhibit higher stiffness and tensile strength, but lower compressive strength due to long fiber buckling. With the developed micromechanics model, the multiaxial elasto-plastic responses of MFSSs are simulated. A macroscopic phenomenological constitutive model with a segmented yield function is proposed to describe the predicted multiaxial responses. The yield function and its evolution can be fully calibrated in terms of the uniaxial tension and compression responses rather than complex multiaxial loading responses, which can greatly facilitate practical applications of the model. This constitutive model is also expected to be applicable to other fiber sintered materials with hydrostatic pressure sensitive and asymmetric tension–compression yielding behaviors.

1. Introduction

Cellular materials with attractive thermal, acoustic, electrical and mechanical properties are promising for a wide range of engineering applications (Ashby et al., 2000; Banhart, 2001; Gibson and Ashby, 1997; Lu et al., 2006). Recent advances in fiber-pullout techniques have promoted the development of a new type of cellular material -MFSSs[1] (Xi et al., 2011). These porous materials consisting of metallic fiber networks can be used as structural materials as the low density core of sandwich panels (Clyne et al., 2005; Markaki and Clyne, 2003a,b; Zhou and Stronge, 2005), in addition to functional materials as anodic gas diffusion backing (Liu et al., 2004), catalyst support (Qiao et al., 2008), and filtration net (Wang, 2003), among others. When used as structural components, they show an attractive combination of properties, such as high specific stiffness and good energy absorption capacity due to the existence of long plateau stress during plastic yielding. To fulfill the structural applications, a mutual understanding of their mechanical properties is essential. So far, however, only limited studies are available (Qiao et al., 2009).

For the mechanical properties of generic cellular solids, extensive studies have been conducted during the past decades. In their monograph, Gibson and Ashby (1997) provided a comprehensive study on the property characterization and

* Corresponding author. Tel.: +86 10 62783488.
E-mail address: chencq@tsinghua.edu.cn (C.Q. Chen).
[1] Abbreviation of porous metal fiber sintered sheets.

0022-5096/$ - see front matter © 2012 Elsevier Ltd. All rights reserved.
http://dx.doi.org/10.1016/j.jmps.2012.08.006

engineering applications of a number of cellular materials, including two dimensional (2D) honeycombs and three dimensional (3D) foams, either natural or man-made. They demonstrated that the relative density (i.e., the ratio of the macroscopic density of a cellular material to that of its constituting solid material) is a key parameter to describe the mechanical properties of cellular materials. Despite the success of this phenomenological study, the models established are difficult to characterize the microstructural morphology with great complexity and experiments are usually required to determine constitutive parameters. Alternatively, micromechanics models are also extensively applied to quantitatively relate the microstructure constitution and macroscopically mechanical properties of porous material, albeit highly porous materials (e.g., metal foams and MFSSs) are macroscopically homogenous but strongly heterogeneous on micro-scales. The generation of a microscopically based macroscopic stress–strain relation from a representative volume element (RVE), which is preferred to the full scale model due to computational limitations, is proposed by some pioneering works, only cited a few (Hashin and Shtrikman, 1963; Hill, 1963, 1965). It is suggested that the macroscopic stress and strain could be identified from the average values of the microscopic corresponding quantities over a RVE. The selected RVE must be periodic, i.e., the microstructure should be periodic repetitions of the RVE and the applied displacement and traction force are periodic and anti-periodic, respectively to meet the continuity and equilibrium between arbitrary two neighboring RVEs.

With the assistance of the finite element method (FEM), some advanced models (Bao et al., 1991; Christman et al., 1989; Michel et al., 1999) are proposed to explore macro-mechanical responses of materials through discretization of a RVE. Although much more complicated RVEs can be modeled, this method also suffers from a few limitations: many porous materials such as Voronoi foams or honeycombs as well as the material investigated in present paper-MFSSs are not microscopically periodic. To resolve this issue, the RVEs composed of a significant number of irregular cells or other types of units are developed to explore the mechanical properties of materials with complex microstructures (Böhm et al., 1993; Michel and Suquet, 1992; Moulinec and Suquet, 1998; Nakamura and Suresh, 1993). With the development of computational techniques, the ratio of the RVE size to the characteristic size of microstructure (e.g., the length of the inclusions or cells) can be significantly increased. In such cases, the computations will be less sensitive to the boundary conditions or its influence would even vanish if the mode size is sufficiently large (Huet, 1990; Jiang et al., 2001). Many micromechanics models of this category are developed to explore the mechanical properties of porous materials with highly irregular microstructures (e.g., two dimensional Voronoi foam and three dimensional porous materials with highly interconnected irregular pores) (Chen et al., 1999; Ghosh and Moorthy, 1995; Roberts and Garboczi, 2002a; Silva and Gibson, 1997; Zhu et al., 2000). Since the irregularity of microstructure of MFSSs is much more remarkable than most of known materials mentioned above, the size of the RVE employed should be first examined to promise that the micromechanically obtained results could accurately represent the overall macroscopic mechanical behavior of the materials. The ratio of the RVE size to the characteristic size of microstructure is expected to be large while the influence of different boundary conditions is expected to be insignificant.

Both phenomenological and micromechanical approaches merged from above presented frameworks are further applied to characterize more detailed and specific mechanical behaviors of porous materials. In order to explain the significant discrepancy between theoretically predicted hydrostatic strength and experimental measurements, several types of imperfection have been studied (Attia et al., 2010; Chen et al., 1999; Gan et al., 2005; Grenestedt, 1998, 1999; Grenestedt and Bassinet, 2000; Meguid et al., 2002; Silva and Gibson, 1997) and their effects on reducing the hydrostatic stiffness and strength in imperfect porous material were discussed. It was contended that the imperfections change the stretching dominated deformation mechanism of cell edges into bending dominated one, resulting in significant decrease of the hydrostatic stiffness and strength. The influence of the deformation mechanism of cell edges on the mechanical properties of perfect metallic foams were studied (Grenestedt, 1999) to give a reference for further works on the imperfection effect. Cell-wall waviness and non-uniform cell-wall thickness which are considered as important imperfections for cellular foams (Chen et al., 1999; Grenestedt, 1998; Grenestedt and Bassinet, 2000) are absent in MFSSs whilst the extent of cell size variation and cell-wall misalignment (Chen et al., 1999; Grenestedt, 1999; Silva and Gibson, 1997) are much more severe in MFSSs than in cellular metallic foams and honeycombs. The influence of spatial density variation on the mechanical properties of metallic foams has been found to be important (Attia et al., 2010; Meguid et al., 2002). Further, according to previous studies, cell size variation and cell-wall misalignment reduce hydrostatic strength and stiffness of cellular foams, because such imperfections usually change the deformation mechanism of cell edges from stretching dominated to bending dominated.

Based on the Maxwell criterion, Deshpande et al. (2001) examined the influence of the connectivity of joints on the deformation mechanism of strut models with regular microstructures. Triangular lattices, Kagome lattices and hexagonal honeycombs with stochastic nodal dispersion were numerically simulated and it was found that nodal connectivity plays an important role in the sensitivity of the mechanical properties to imperfections (Symons and Fleck, 2008). It should be noted that such regular microstructures with morphological imperfections are significantly different from the purely random microstructures of MFSSs, as all joints in the latter have 4 struts while the cells with different shapes are composed of unknown number of struts (edges). Thus, for MFSSs, the deformation mechanism of cell edges cannot be simply and solely determined by the Maxwell criterion.

To describe the initial yield surface and subsequent plastic flow rules, several constitutive models of cellular materials have been proposed. Drucker and Prager (1952) established a hydrostatic pressure sensitive model with one more parameter than the Mises criterion for materials with different tensile and compressive strengths. In this model, the hydrostatic pressure sensitiveness depends on the ratio of tensile strength to compressive strength, which is not suitable

for cellular materials in which even if the tensile and compressive strengths are identical, the sensitiveness of hydrostatic strength to yielding still exists. Based on theoretical analysis, a pressure sensitive model with identical tensile and compressive strength was proposed by Gibson and Ashby (1997) for perfect foams. However, because morphological imperfections are not considered in this model, the hydrostatic strength is overestimated. Zhang et al. (1997) and Miller (2000) considered both the hydrostatic pressure sensitiveness and the difference between tensile and compressive strengths as two independent factors and proposed a three-parameter yield function of elliptical shape in the equivalent stress and mean stress plane. The difference between the two models lies in that the plastic flow in the work of Zhang et al. is characterized in terms of the volumetric strain whereas that in the model proposed by Miller is governed by the uniaxial compressive response and volumetric strain. Deshpande and Fleck (2000) proposed a constitutive model governed by either isotropic hardening or differential hardening, with the initial yield surface characterized by the plastic Poisson ratio. Wang and Pan (2006) proposed a non-quadratic yield function and found that it well characterizes the experimentally measured yielding behavior of polymeric foams under multi-axial loading. Chen and Lu (2000) proposed a general constitutive model for both incompressible and compressible materials by introducing characteristic stress and characteristic strain and successfully applied the model to describe the multi-axial yielding behavior of metallic foams. With the development and increasing applications of various types of porous material, several constitutive models have also been proposed to characterize their anisotropic and visco-plastic behaviors (Alkhader and Vural, 2009, 2010; Hård af Segerstad et al., 2008; Tsuda et al., 2010). Whilst the constitutive models mentioned as above have been proved to be effective in predicting the mechanical behavior of porous materials (Meguid et al., 2004). Segerstad et al. (2008) developed a constitutive model to describe the tension–compression asymmetry in two dimensional open cell foams due to the buckling of cell edges. The buckling feature of cell edges is also observed in MFSSs, owing to the existence of long fibers. The single-strut approach used in the model by Segerstad et al. can reduce computational cost and simplify the modeling of the plasticity, viscoelastic and damage of the cell edges. However, MFSSs have highly irregular microstructures and widely dispersed direction and length of the fibers, as compared to open cell metal foams. Application of the model by Segerstad et al. has yet to be verified. Indeed, a phenomenological constitutive model that can account for the complex behaviors and microstructures inherent in MFSSs is desirable.

Application prospect, limited existing studies, and significant differences from traditional porous materials such as metallic foams and honeycombs call for a specific numerical simulation model to describe the mechanical behavior of MFSSs. Such a model is proposed in the present investigation. To begin with, the methodology of constructing a random fiber felt model is introduced; several factors in the model which may lead to unexpected influences on the simulation results or cause errors are excluded. The model is subsequently applied to obtain the elastic constants of Young's modulus, bulk modulus, and Poisson ratio for various relative densities. With the large deflection effect accounted for in non-linear plastic simulations, the predicted stress versus strain curve indicates significant difference between tension and compression beyond the initial linear elastic regime. For selected relative densities, the initial yielding behaviors of a MFSS are described by numerically calculating its uniaxial tensile strength, uniaxial compressive strength, hydrostatic tensile strength, hydrostatic compressive strength as well as initial yield surface in the equivalent stress versus mean stress plane based upon the non-linearity of its characteristic stress versus characteristic strain responses. Further, a 2D phenomenological constitutive model is proposed to describe its plastic flow rule.

2. Simulation method

2.1. Random beam model

A random strut numerical model based on the microstructure of typical MFSSs is presented in this section, which is significantly different from previously established 2D and 3D numerical models for porous material in terms of the cell shape and the joint structure (Luxner and Pettermann, 2009; Luxner et al., 2009; Roberts and Garboczi, 2002b). The numerical model is based on the microstructure of MFSS specimens used in experiments (Zhao, 2011)[2]. The MFSSs consisting of sequentially overlapped 316L stainless steel fiber layers are produced by sintering in a vacuum thermal processing furnace at $\sim$1500 °C, with properly selected external pressure applied (Xi et al., 2011). As the sintered fibers within each layer are randomly arranged, macroscopically speaking, the MFSSs thus processed are transversely isotropic, the plane of the layers being the isotropic plane. In the following, the direction perpendicular to the isotropic plane is referred to as the thickness direction or the out-of-plane direction. A SEM (scanning electron microscope) image showing the isotropic in-plane of a typical MFSS sample is presented in Fig. 1(a). The experimental results of Zhao (2011) indicate that the in-plane stiffness and strength of the MFSSs are much higher than those in the thickness direction. In addition, the Poisson ratio in the thickness direction is close to 0, which implies that the deformations in the isotropic plane and in the thickness direction are approximately independent of each other. It is thus desirable to develop a 2D model to simulate the in-plane elasto-plastic behavior of MFSSs. To this end, a 2D micromechanics random beam model is developed, with a typical model shown in Fig. 1(b). Comparison between Fig. 1(a) and (b) reveals that the generated microstructure of the developed random beam model is indeed very similar to that of real MFSSs. Details of the model construction are discussed as follows.

[2] Materials provided by the State Key Laboratory of Porous Metal Materials, Xi'an, PR China.

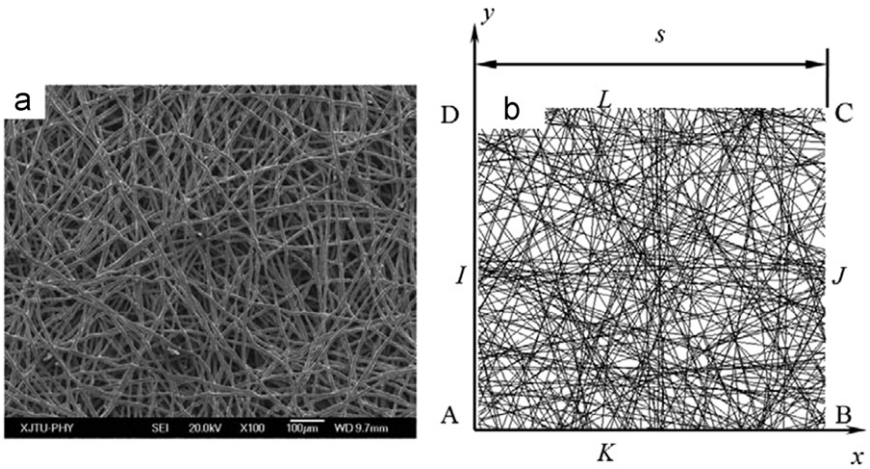

Fig. 1. (a) The SEM image of a porous metal fiber sintered sheets with fiber diameter 8 μm and relative density 0.25; (b) typical random beam model for porous metal fiber sintered sheets (MFSSs).

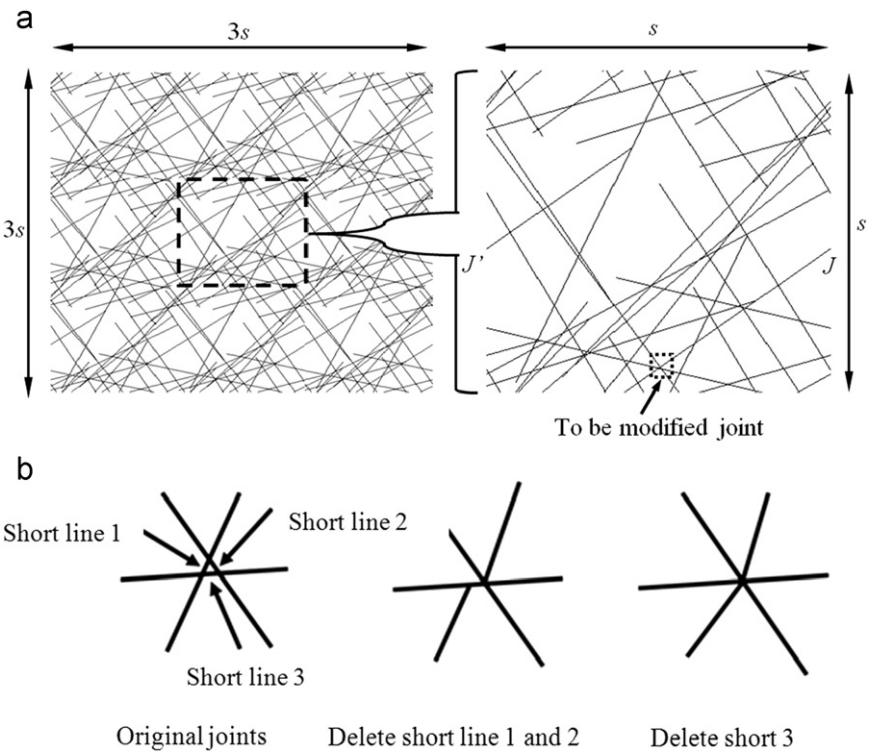

Fig. 2. Illustrations of (a) how to construct a periodic model for porous metal fiber sintered sheets and (b) how to remove exceedingly short beams in the original model. Note that the model shown in (a) is only for the illustration purpose. The models used in simulations have much more fibers as shown in Fig. 1(b).

The geometrical microstructure of the random beam model is generated by overlapping randomly distributed straight lines of length l representing the fibers in MFSSs. Although the microstructures in the model are randomly distributed, the model itself should be periodic (i.e., repetitive in the x–y plane) to ensure its prediction to be representative of MFSSs. For a better illustration of how the periodicy of the model is guaranteed, a model with a few of lines is shown in Fig. 2(a). A set of randomly distributed fibers of length l and with periodicy of s in the x and y directions is first generated within a space of size $3s \times 3s$. The central points and directions of the fibers are randomly generated following the uniform distribution rule. Then, a model with dimensions $s \times s$ (as denoted by the broken lines in Fig. 2(a) with $l=1.6s$) can be obtained by deleting all the segments of the lines out of the broken lines. From the corresponding pairs of nodes along opposite boundaries (e.g., J and J' in Fig. 2(a)), it is easily seen that the resulting model is periodic. The effect of the fiber length l upon the predicted mechanical properties will be discussed in Section 2.2.

The ideal bonding (i.e., rigid connection) at the intersection joints between fibers is assumed. It is noted that intersection of randomly overlapped fibers may produce extremely short segments, causing convergence issues during numerical computation. To avoid this, all fibers in the model are carefully examined. Any fiber is deleted if its length is less than one fifth of the average value, with other fibers connected to the two joints of the deleted line directly converged at one joint. An example is shown in Fig. 1(b) as to how to remove the extremely short segments marked in Fig. 1(a) from the micromechanics model, e.g., any fiber shorter than fiber thickness will be removed. It has been established that whilst the deletion of these short segments has negligible influence on the predicted mechanical responses of MFSSs, it can greatly improve the computation efficiency.

The finite element method (FEM) is employed to simulate the stress versus strain responses of the random beam model constructed following the procedures outlined above. The fibers are meshed using Timoshenko shear deformable 2-node-beam elements of width 12 μm, which is also the diameter of the fibers used in MFSS specimens for supporting experiments presented later (Zhao, 2011). Large deformation option is enabled in the simulations to explore the nonlinear yielding and buckling of the fibers. It should be pointed out that, although out of plane buckling is possible in real materials it cannot be captured in the developed 2D models. The constituting solid material of the fibers is assumed to be elastic perfectly plastic with Young's modulus $E_s=210$ GPa, Poisson ratio $\nu=0.3$ and yielding strength of $\sigma_s=290$ MPa, typical for 316L stainless steel. The mass density of the generated model is given by:

$$\rho_r = \rho_s \frac{t\sum l}{s^2} \tag{1}$$

where t, l and ρ_s represent the width (unit thickness), length and mass density of the fibers, respectively. In the following simulations, ρ_r is varied by changing $\sum l$ and s but fixing t and ρ_s.

To explore the mechanical properties of MFSSs, both uniaxial and proportionally biaxial straining loadings are applied to the random beam model. In the following sections, σ_x, σ_y ,ε_x and ε_y not only denote the macroscopic stresses and strains in the x and y directions but also the principal stresses and strains, since only tension or compression without shearing is imposed on the boundaries along the x or y axis. Three different boundary conditions (i.e., periodic boundary condition; prescribed displacement boundary condition with rotation constraint, corresponding to non-zero stress couples; and prescribed displacement boundary condition without rotation constraint, corresponding to zero stress couples) are considered and discussed in Section 0 (Chen et al., 1999). To describe how different boundary conditions are imposed upon the periodic structure of Fig. 1(b), we define I and J as a pair of opposite nodes on boundaries AD and BC; similarly, K and L as a pair of opposite nodes on boundaries AB and DC. Under proportionally biaxial straining, the prescribed displacement boundary condition without rotation constraint requires that the translation displacements u_x^I (displacement of node I in x direction), u_x^J, u_y^K, and u_y^L at I, J, K, L satisfy:

$$u_x^I = u_y^K = 0,\ u_x^J = s\varepsilon_x,\ u_y^L = s\varepsilon_y \tag{2}$$

where ε_x and ε_y are separately the macroscopic average strains in the x and y directions. The prescribed displacement with rotation constraint is the combination of Eq. (2) and the following Eq. (3):

$$\theta^I = \theta^J = \theta^K = \theta^L = 0 \tag{3}$$

where θ^I, θ^J, θ^K, and θ^L are the rotations at I, J, K, L, respectively. Periodic boundary conditions imply:

$$u_x^J - u_x^I = s\varepsilon_x,\ u_y^L - u_y^K = s\varepsilon_y,\ \theta^J - \theta^I = \theta^L - \theta^K = 0. \tag{4}$$

Uniaxial loading is similarly defined, with the constraint on free stress boundaries released.

The macroscopic stresses are calculated as (Chen et al., 1999):

$$\sigma_x = \frac{1}{s^2}\sum x^J F_x^J$$
$$\sigma_y = \frac{1}{s^2}\sum y^J F_y^J \tag{5}$$

where F_x^J and F_y^J are the reaction forces of node J, x and y are the coordinates of node J, and summation is carried over the boundary ABCDA.

2.2. Mesh sensitivity and error analysis

Recall that the beams in the model are generated randomly and only a finite number of beams are employed due to computation limitation. It is therefore necessary to perform mesh and model size sensitivity studies as well as error analysis of the FEM simulation results inherent to the random structures. In this section, five factors relevant to meshing dependence (i.e., model size, length of initial beams, different types of boundary condition, and randomness of microstructure) that may have significant effects on the simulation results are examined.

Element size is chosen according to the relative density, which is dependent upon the length of each cell edge. From the results of a series of preliminary models, it is found that finite elements having the size of about one second of the fiber width are small enough to give convergent results. This criterion is applied throughout subsequent simulations.

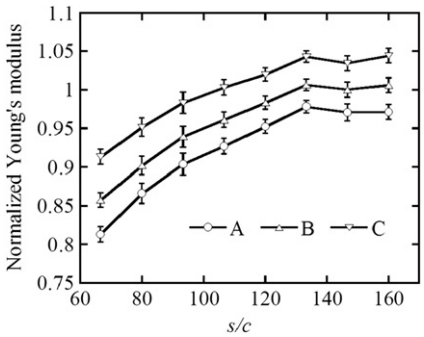

Fig. 3. Model size dependence upon the Young's modulus of a porous metal fiber sintered sheets with relative density of 0.20. Three different boundary conditions (A) periodic, (B) prescribed displacement conditions without rotation constraint and (C) prescribed displacement conditions with rotation constraint) are considered and over 20 random models are used to obtain 95% confidence intervals for each model size (c is the averaged cell size). The results are normalized by the values obtained from no rotation boundary condition and $s/c=146$.

Because all numerical models are established randomly, their elasto-plastic responses are expected to show difference even if they are generated using identical parameters (such as relative density, length of initial beams and model size). Although increasing the ratio of model size to cell size can reduce and may even eliminate such variance, it would be unacceptably computationally inefficient. Similar problems exist in other numerical simulations of porous materials (Wicklein and Thoma, 2005). Thus, it is desirable to use an effective method to present reliable results from dispersed data due to the randomness of the numerical models used in the present study. Here, the interval estimation method (Rice, 2007) is used to provide the estimation intervals of the mechanical properties obtained from the dispersed results of the random models. The mechanical properties obtained from 10 to 20 random models are post-processed to assure that the estimation of 95% confidence interval associated with the mean values is below 5% for the elastic constants and 8% for the plastic properties.

Theoretically, the dependence of the simulation results upon model size will diminish if the model size compared to the cell size is sufficiently large. However, according to the numerical simulations of Chen et al. (1999), the necessary size to give convergent results for MFSSs is much larger due to the irregularity of their microstructures. Their results suggest that when the ratio of model size to averaged cell size reaches 20, the size effect is negligible for Alporas aluminum foams. Here, we simulate several groups of models and post-process the results with the interval estimation method to find the size required for convergence. Fig. 3 shows the simulated Young's modulus as a function of the normalized model size (s/c) for three different boundary conditions, where c is the averaged cell size defined by $c^2=s^2/N_c$, with N_c being the total number of cells within the model. Such a definition of the averaged cell size c is based upon the assumption of an equivalent regular square honeycomb with the same number of cells, cell wall thickness, and relative density. The cell edge length of the equivalent square honeycomb is adopted to be the averaged cell size c of the random beam model. It is found that the Young's modulus does not change as the model size exceeds 140 times the averaged cell size c. Such a big model size in order to ensure numerical convergence is due to significant cell shape and size variance in MFSSs as compared to Voronoi foams, which also increases the deviation of simulation results. The results of Fig. 3 also demonstrate that the model size used in this paper (140 times the averaged cell size) is big enough to reduce the boundary effects to a negligible scale (e.g., the difference in the converged results for different boundary conditions less than 5%). Since the model size is given in terms of averaged cell size, for lower relative density, larger model size should be employed due to increasing of averaged cell size. Note that the prescribed displacement conditions without rotation constraints, compared to the periodic boundary conditions are usually closer to the loading conditions (e.g., uniaxial loading) in most experiments and are easier to be implemented into the random beam models. Therefore, although Chen et al. (1999) showed that periodic boundary conditions are more appropriate for Voronoi foam models, the prescribed displacement boundary conditions without rotation constraint are employed in the following random beam model simulations. In addition, the effect of the fiber length l upon the predicted mechanical properties is explored and is found that, when the fiber length (l) in the numerical models is as large as about 220 times the averaged cell size c, convergence of the numerical results is guaranteed. It is also noted that the length of fibers used in experiments (Zhao, 2011) are much longer than the convergent length estimated above and are found have little influence on measured results. The geometrical models for all FEM simulations in the following sections are generated according to the parameters discussed above.

3. Numerical results

3.1. Elastic constants

Fig. 4 presents the numerically simulated stress versus strain responses of MFSSs subject to uniaxial loading and biaxial loading of proportional straining $\varepsilon_x:\varepsilon_y=1:1$, $-1:-1$, and $1:-1$ (i.e., corresponding to equi-biaxial tension, equi-biaxial compression and deviatoric straining loading). These curves exhibit typical features of elasto-plastic responses: a linear

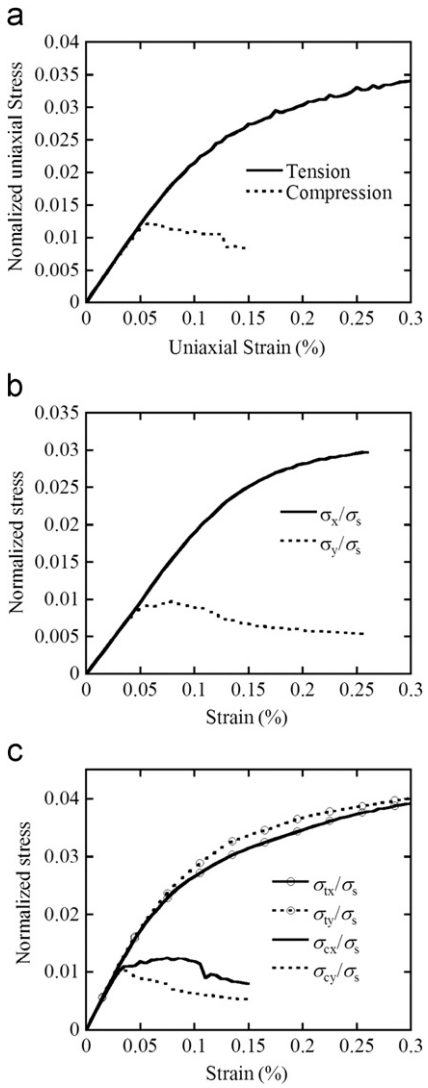

Fig. 4. Simulated stress normalized by the yield strength of the fibers versus strain responses of a porous metal fiber sintered sheets with relative density of 0.15 under (a) uniaxial tension and compression, (b) deviatoric strain loading, and (c) equi-biaxial tension (σ_{tx}/σ_s,σ_{ty}/σ_s) and compression (σ_{cx}/σ_s,σ_{cy}/σ_s).

elastic regime followed by non-linear stress hardening under tension whereas lower yielding stress and subsequent slight softening under compression. The lower compressive strength than tensile strength is related to the non-linear buckling effect under compression when large-deflection effects are considered. The elastic constants (i.e., Young's modulus, bulk modulus and Poisson ratio) of MFSSs are calculated from the predicted stress versus strain curves and their dependence upon the relative density is shown in Fig. 5. It is seen that both the Young's modulus and bulk modulus depend almost linearly upon the relative density. Curve fittings give the following approximate relationships:

$$\frac{E^*}{E_s} = 0.259\rho_r \tag{6}$$

$$\frac{\kappa^*}{E_s} = 0.183\rho_r \tag{7}$$

where E^*/E_s is the macroscopic Young's modulus of MFSSs normalized by that of the solid cell edges (beams), κ^*/E_s is the normalized bulk modulus and ρ_r is the relative density. The experimentally measured in-plane Young's modulus in Fig. 5(a) are taken from Zhao (2011). The present model predictions agree very well with experimental measurements though the simulation results are slightly larger: this may be attributed to the fact that various morphological imperfections of the test specimens are not included in the random beam model. As for the Poisson ratio, it is seen from Fig. 5(b) that the prediction is close to 0.3 (between 0.24 and 0.32) for relative density ranging from 0.05 to 0.25. We note from Zhao (2011) that the measured in-plane Poisson's ratio of a MFSS with ρ_r=23% is 0.23. Again, good agreement

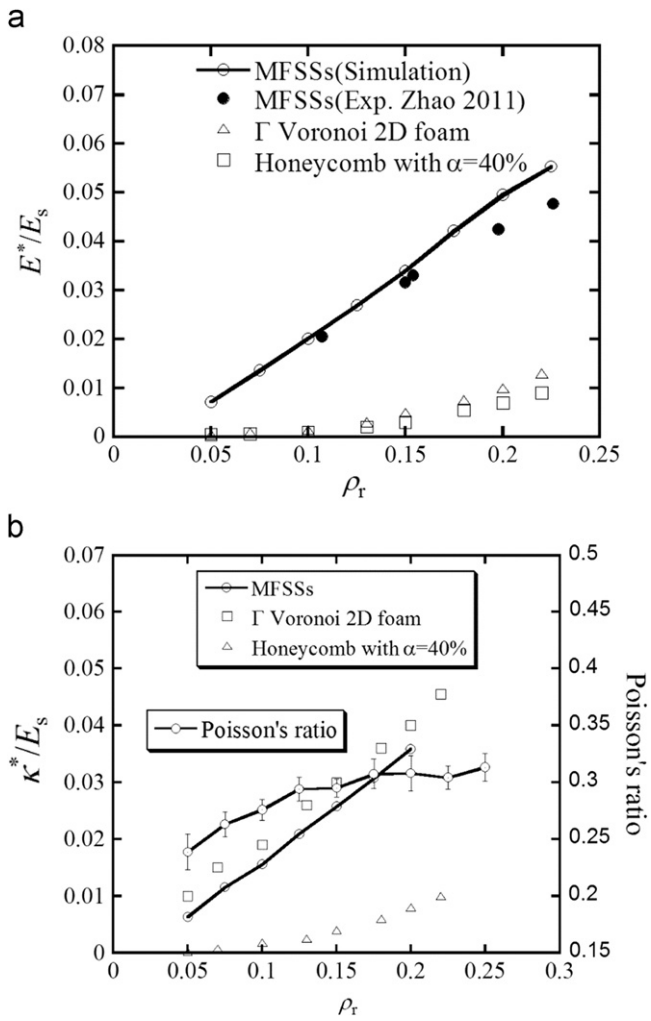

Fig. 5. Dependence of (a) Young's modulus and (b) bulk modulus and Poisson ratio of porous metal fiber sintered sheets compared with the Young's modulus and bulk modulus of Γ-distributed Voronoi 2D foam without imperfections and honeycomb with $\alpha=40\%$ (representing significant cell edge misalignment) from numerical simulations(Chen et al., 1999). Predicted data points are marked by symbols, with lines used for eye guide only.

between model prediction and experimental result is achieved. The results for Voronoi 2D foams and honeycombs (Chen et al., 1999) are also included in Fig. 5. The normalized Young's modulus of the MFSSs is significantly higher than that of either Γ-distributed Voronoi 2D foams without imperfections or honeycombs with $\alpha=40\%$ (indicating significant cell edge misalignment). In comparison, the normalized bulk modulus of the MFSSs is similar to that of Γ-distributed Voronoi 2D foams without imperfections.

3.2. Yield strength

Traditionally, the yielding of a material is defined according to the von Mises equivalent stress versus strain curve. However this method is not suitable for hydrostatic sensitive materials subject to hydrostatic loading in which the Mises equivalent stress is zero. Another commonly used mean stress versus volumetric strain curve cannot be used universally either (e.g., it is not applicable to pure shear loading). On the contrary, the characteristic strain $\overline{\varepsilon}$ and stress $\overline{\sigma}$ (Chen and Lu, 2000) are able to provide a consistent ways to define yielding under various loading conditions (e.g., uniaxial, equi-biaxial static, pure shear, etc.). The definition of yielding is then based on the plastic portion of the characteristic strain. Following Chen and Lu (2000), the characteristic stress and strain,$\overline{\sigma}$ and $\overline{\varepsilon}$, are expressed as:

$$\overline{\sigma}^2=\sigma_e^2+\beta^2\sigma_m^2$$

$$\overline{\varepsilon}^2=\varepsilon_e^2+\frac{\varepsilon_v^2}{\beta^2} \tag{8}$$

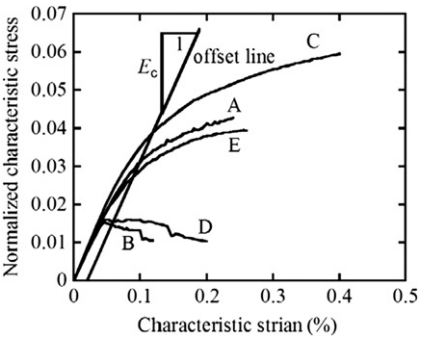

Fig. 6. Simulated characteristic stress normalized by the yield strength of the fibers versus strain responses of a porous metal fiber sintered sheets with relative density of 0.15 subjected to uniaxial tension (A), uniaxial compression (B), equi-biaxial tension (C), equi-biaxial compression (D) and deviatoric loading with $\varepsilon_x:\varepsilon_y=1:-1$ (E).

where

$$\begin{aligned} \sigma_e &= \sqrt{(\sigma_x-\sigma_y)^2} \quad \sigma_m = \tfrac{\sigma_x+\sigma_y}{2} \\ \varepsilon_e &= \sqrt{\tfrac{1}{4}(\varepsilon_x-\varepsilon_y)^2} \quad \varepsilon_v = (\varepsilon_x+\varepsilon_y) \end{aligned} \tag{9}$$

Notice that the definition (8) can be extended to anisotropic materials (Alkhader and Vural, 2009).

In the elastic regime, the relationship between $\overline{\varepsilon}$ and $\overline{\sigma}$ satisfies:

$$\overline{\sigma} = E_c\overline{\varepsilon} \tag{10}$$

where

$$\begin{aligned} \beta &= 2\sqrt{\frac{1-\nu}{1+\nu}} \\ E_c &= \frac{2E}{1+\nu} \end{aligned} \tag{11}$$

With Eq. (8), the predicted stress–strain curves for several different loadings are re-plotted in terms of their normalized corresponding characteristic stress and strain; see Fig. 6. It is seen that the yielding of the MFSSs can be defined consistently by introducing the 2D characteristic strain $\overline{\varepsilon}$ and stress $\overline{\sigma}$. The results of Fig. 6 show that all curves collapse onto a master curve in the elastic regime and comply with Eq. (10) while they differ from each other in the plastic regime. The plastic portion of the characteristic strain is given by:

$$\overline{\varepsilon}_{\mathrm{p}} = \overline{\varepsilon} - \frac{\overline{\sigma}}{E_{\mathrm{c}}} \tag{12}$$

Once $\overline{\varepsilon}_p$ reaches the prescribed offset value, the yielding is defined. The characteristic stress versus characteristic strain curves are then used to define the yield strength, initial yield surface, and its subsequent evolution.

Even though the solid material constituting the MFSSs is modeled as elastic-perfect-plastic, strain hardening effect of the MFSSs is remarkable in tension due to their serious cell size and cell shape variance (see Fig. 4). It is thus not surprising that different yield strengths will be obtained if different offset values are used to define yielding. The sensitivity of yield strength and yield surface upon selected offset values of strain might bring troubles in the comparison of results, such as 0.3% (Deshpande and Fleck, 2000), 0.1% (Wicklein and Thoma, 2005) and the traditional value for solid material (0.2%) in experimental studies as well as 0.01% (Alkhader and Vural, 2009) chosen for theoretical studies. Usually, it is preferable to use relatively larger offset values in experimental studies and smaller values in numerical simulations or theoretical analyses. In present paper, the offset value of 0.02% is adopted.

According to the definition presented above, the yield strength versus relative density curves of the MFSSs are obtained and presented in Fig. 7. For comparison, the experimental results on the uniaxial tensile strength of the MFSSs (Zhao, 2011) are also shown Fig. 7(a). The predicted results are slightly lower than the experimental ones, which is mainly attributed to the larger offset strain value (0.2%) employed in the experimental study (Zhao, 2011) than that used in the present theoretical investigation (0.02%). Nevertheless, the overall agreement between theory and experiment is very good. Recall that the considered MFSSs are transverse isotropic and their deformations in the isotropic plane and in the thickness direction are approximately independent of each other. A 2D model is believed to be adequate for their in plane behaviors. It is seen from Fig. 1 that the developed 2D random beam models are very similar to the in plane microstructures of MFSSs. With proper material parameters and boundary conditions employed, it is thus not too surprising that a good agreement is achieved between the model predictions and available experimental results for the in plane stiffness, Poisson's ratio and yield strength (as shown in Figs. 5 and 7).

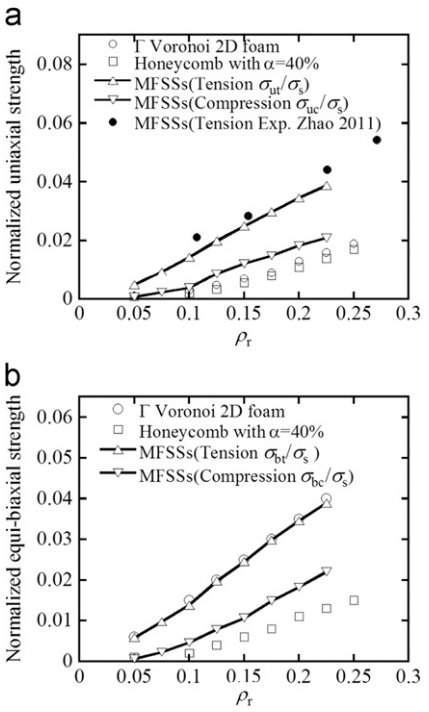

Fig. 7. Normalized (a) uniaxial strength and (b) equi-biaxial strength of porous metal fiber sintered sheets plotted as functions of relative density. For comparison, the results for Γ-distributed Voronoi 2D foam without imperfections and honeycomb with $\alpha=40\%$ (representing significant cell edge misalignment) from numerical simulations (Chen et al., 1999) are also included. Predicted data points are marked by symbols, with lines used for eye guide only.

With reference to Fig. 7, the curve fitted results are given as follows:

$$\frac{\sigma_{ut}}{\sigma_s} = 0.163\rho_r \tag{13}$$

$$\frac{\sigma_{uc}}{\sigma_s} = 2.6246\times10^{-3}\rho_r + 4.6555\times10^{-1}\rho_r^2 \tag{14}$$

$$\frac{\sigma_{bt}}{\sigma_s} = 0.161\rho_r \tag{15}$$

$$\frac{\sigma_{bc}}{\sigma_s} = -7.5454\times10^{-4}\rho_r + 4.7376\times10^{-1}\rho_r^2 \tag{16}$$

where σ_{ut}, σ_{uc}, σ_{bt}, σ_{bc} are the uniaxial tensile strength, uniaxial compressive strength, equi-biaxial tensile strength and equi-biaxial compressive strength, respectively. Similar to the elastic constants, the uniaxial and equi-biaxial tensile strengths increase linearly with the relative density whereas the compressive strengths are higher order functions of the relative density.

For different loading cases, it is now widely accepted that the mechanical properties of porous materials are dictated by their microstructures via the deformation mechanisms of cell ligaments/edges. In the numerical simulations, the deformation mechanisms of cell edges can be inferred from the relationship between the mechanical property and the relative density. If the tensile loading is applied along the direction parallel to the fibers, the stretching dominated deformation of the cell edges implies that (Gibson and Ashby, 1997; Grenestedt, 1999):

$$\frac{E^*}{E_s} = \frac{\sigma_y^*}{\sigma_s} = \frac{1}{2}\rho_r \tag{17}$$

In comparison, if the angle between the tensile loading and the fibers is 45 degree, the bending dominated deformation of the cell edges implies that:

$$\frac{E^*}{E_s} = \frac{1}{4}\rho_r^3 \tag{18}$$

It is noted that the relationships between the tensile mechanical properties and relative density of the MFSSs (Figs. 5 and 7) follow linear relationships when the relative density is greater than 0.1, suggesting stretching dominated mechanism with respect to Eq. (17). Under both equi-biaxial and uniaxial compressions, buckling of the cell edges is

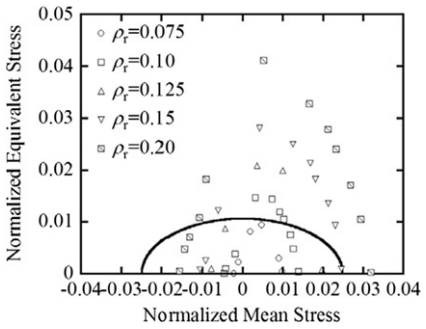

Fig. 8. Predicted initial yield surfaces of porous metal fiber sintered sheets normalized by yield strength of steel fibers for selected relative densities (0.075, 0.1, 0.125, 0.15, and 0.2, denoted by symbols). For comparison, the normalized yield surfaces of Γ-distributed Voronoi 2D foam with relative density of 0.15 (Chen et al., 1999) is included as solid line.

predicted for MFSSs, also implying stretching dominated deformation mechanism. In view of the above arguments, one may conclude that, for MFSSs, the deformation mechanism of the cell edges is stretching dominated.

The asymmetry in tensile and compressive strengths is evident from Fig. 7. Similar feature has been found in the experimental study of metallic foams (Deshpande and Fleck, 2001). For the MFSSs considered here, the difference is more pronounced owing to the existence of long beams (fibers) which are prone to buckling. Indeed, for low relative densities, the buckling effect is believed to be more pronounced so that MFSSs with low relative densities should not be used to withstand compressive loading.

3.3. Yield surface and its evolution

From the simulated multiaxial stress versus strain curves, the yield surface and its evolution can be explored. Fig. 8 presents the initial yield surfaces in the equivalent stress versus mean stress plane for MFSSs with different relative densities, denoted by various symbols. For comparison, the numerically simulated yield surface of Γ-distributed Voronoi 2D foams with relative density 0.15 (Chen et al., 1999) is included as solid line. The results of Fig. 8 demonstrate that the compressive strengths are much lower than the tensile strengths. In the tension dominated regime, the MFSSs have remarkably higher strength than that of Voronoi 2D foams. However, such a difference vanishes if the yield point lies on mean stress axis, as expected, because it has been established that the cell edges of Voronoi 2D foams are relevant to stretching under equi-biaxial macroscopic loading and relevant to bending under uniaxial macroscopic loading (Chen et al., 1999).

In addition to the dependence of initial yield surfaces upon relative density as shown in Fig. 8, the post yield surfaces (i.e., yield surface evolution) are also of great interest from theoretical and practical points of view. It should be pointed out that, the present numerical simulations do not consider contact between adjacent cell edges (fibers) under compression, and hence the stress versus strain curves exhibit softening following initial yielding (see Figs. 4 and 6) which is not observed in experiment (Zhao, 2011). Actually, under compression, the contact between fibers inevitably leads to hardened elasto-plastic response before densification. Thus, we assume that the compressive stress remains constant after reaching the peak value despite its slight decreasing with waving from the simulated results. Under the assumption that the yield surface is not extendable in the compression dominated regime, the random beam model predicted yield surfaces and their evolution are plotted in Fig. 9(a) and (b) (denoted by symbols), respectively, for MFSSs with selected relative densities (0.15 and 0.2). It can be seen that the yield surface in the tensile portion evolves in a geometrically similar manner as the characteristic plastic strain increases from 0% to 0.06%. The solid lines in Fig. 9 represent theoretical model predictions, as will be discussed in the following section.

4. Two dimensional constitutive model for MFSSs

The MFSSs are transversely isotropic with nearly zero Poisson ratios ν_{31} and ν_{32} (3 implying the thickness direction; (Zhao, 2011)), which means their in-plane mechanical behaviors are nearly independent of the deformation in the thickness direction. Accordingly, we propose here a 2D constitutive model for the in-plane stress versus strain responses of MFSSs. To this end, it is observed from Fig. 9 that, in the equivalent stress versus mean stress plane, the yield points in the compression dominated regime comply with a straight line. In the tension dominated area, however, the yield surfaces are elliptical and evolve in a self-similar manner as the characteristic strain is increased. Consequently, a segmented yield function for the 2D in-plane behavior of MFSSs is proposed as:

$$\Phi_1 = -\frac{\sigma_m}{\sigma_{uc}} + \frac{\sigma_e}{2\sigma_{uc}} - 1 = 0 \tag{19}$$

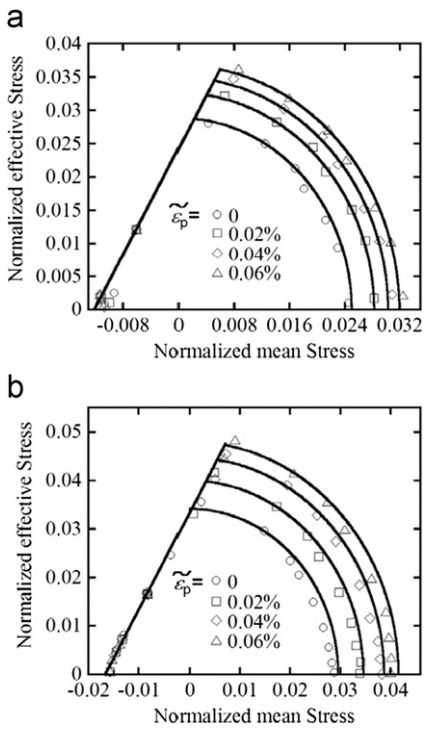

Fig. 9. The yield surface of a porous metal fiber sintered sheets with relative density of (a) 0.15 and (b) 0.2 at selected characteristic plastic stains of 0 (initial yielding), 0.02%, 0.04%, and 0.06%. Lines represent constitutive model predictions from Eqs. (19) and (20) while symbols denote numerical simulation results from the random beam model.

for the compression dominated regime and

$$\Phi_2 = \frac{\sigma_m^2}{A^2} + \frac{\sigma_e^2}{B^2} - 1 = 0 \tag{20}$$

for the tension dominated regime. The intersection of the two functions ((19) and (20)) produces a vertex on the yield surface. The material parameters σ_{uc} in (19) and A and B in (20) are functions of the relative density and/or the characteristic plastic strain, the latter composed of both volumetric plastic strain and equivalent plastic strain according to Eq. (8).

Note that the yield surface Φ_1 is not expandable in the compression dominated regime (see Fig. 9 and relevant arguments in the previous section). The compressive strength σ_{uc} is dependent upon the relative density and independent of the characteristic strain and can thus be calibrated by the uniaxial compressive strength of MFSSs, i.e., Eq. (14) together with Eq. (8). From the plastic characteristic stress versus strain curve under uniaxial tension, A and B in (20) can be calibrated as:

$$A = \sigma_{ut}(\bar{\varepsilon}_p)^2, B = \frac{4}{3}\sigma_{ut}(\bar{\varepsilon}_p)^2 \tag{21}$$

Substitution of (21) into (20) leads to:

$$\Phi_2 = \sigma_m^2 + \frac{3}{4}\sigma_e^2 - \sigma_{ut}(\bar{\varepsilon}_p)^2 = 0 \tag{22}$$

where $\sigma_{ut}(\bar{\varepsilon}_p)$ is a function of the characteristic plastic strain $\bar{\varepsilon}_p$ and $\sigma_{ut}(\bar{\varepsilon}_p)$ equals the initial yield strength when $\bar{\varepsilon}_p = 0$. Since Φ_1 cannot evolve toward the normal direction (perfect elasto-plastic), we assume that the evolution of Φ_2 will only extend the yield surface along the tangent direction, which is consistent with the plasticity theory of Koiter (1960) for multi-yield surface constitutive models. The plastic strain is given by:

$$\dot{\varepsilon}_{ij}^p = \dot{\lambda}\frac{\partial \Phi_2}{\partial \sigma_{ij}} \quad i = 1,2 \tag{23}$$

where the proportionality factor $\dot{\lambda}$ is determined from the consistence condition of plasticity, as:

$$\dot{\Phi}_2 = \frac{\partial \Phi_2}{\partial \sigma_{ij}}\dot{\sigma}_{ij} + \frac{\partial \Phi_2}{\partial \bar{\varepsilon}^p}\dot{\bar{\varepsilon}}^p = \frac{\partial \Phi_2}{\partial \sigma_{ij}}\dot{\sigma}_{ij} + \frac{\partial \Phi_2}{\partial \bar{\varepsilon}^p}\frac{\partial \bar{\varepsilon}^p}{\partial \bar{\varepsilon}_{ij}^p}\dot{\bar{\varepsilon}}_{ij}^p = 0 \quad i = 1,2 \tag{24}$$

Here, for convenience, Einstein summation convention is applied with the assumption that 1 represents the x direction and 2 represents the y direction.

To validate the 2D constitutive model presented above, the predicted yield surface and its evolution for MFSSs with selected relative densities are compared in Fig. 9 with the numerical simulation results from the random beam model. From Eqs. (8) and (13), one gets the uniaxial tensile yield strength.

$$\frac{\sigma_{\mathrm{ut}}(\bar{\varepsilon}_p)}{\sigma_s} = 0.0256 + 0.1394\bar{\varepsilon}_p - 0.585\bar{\varepsilon}_p^2 \tag{25}$$

for MFSS with $\rho_r = 0.15$ and

$$\frac{\sigma_{\mathrm{ut}}(\bar{\varepsilon}_p)}{\sigma_s} = 0.0328 + 0.2060\bar{\varepsilon}_p - 0.8099\bar{\varepsilon}_p^2 \tag{26}$$

For $\rho_r = 0.2$. Correspondingly, the uniaxial compressive yield strengths are obtained as $\sigma_{\mathrm{uc}} = 3.5329$ MPa for $\rho_r = 0.15$ and 5.2979 MPa for $\rho_r = 0.2$. The segmented yield surface and it evolution for MFSSs can thence be fully determined, as shown in Fig. 9 as solid lines. The predictions from the constitutive model are found to agree well with those from the random beam model for both relative densities.

5. Conclusions

The mechanical behavior of porous metal fiber sintered sheets is investigated with a two dimensional micromechanics random beam model. A statistical method is employed to provide an estimation of the interval of 95% credence of the simulation results from the developed model. Convergence of the predictions is guaranteed if the model size exceeds 140 times of the averaged cell size. The model is subsequently used to simulate the in-plane multiaxial stress versus strain curves of MFSSs and predict the dependence of the elastic constants (Young's modulus, Bulk modulus, and Poisson ratio) and yield strength upon the relative density. The predictions agree well with available experimental results. It is demonstrated that the Young's modulus and uniaxial tensile yield strength of MFSSs are much higher than those of Γ-distributed 2D Voronoi foams and honeycombs with similar degree of morphological defects and depend linearly upon the relative density, indicating that the deformation mechanism of fiber stretching rather than bending prevails in MFSSs.

In addition to the elastic and plastic constants, the initial yield surface of MFSSs and it evolution are found to be asymmetrical with respect to tension and compression. In the tension dominated regime of the von Mises equivalent stress versus mean stress plane, the yield surface is elliptical in shape and expands in a self-similar manner, whilst it follows a straight line and is not expandable in the compression dominated regime. Accordingly, an elastoplastic constitutive model is proposed. The model can be fully calibrated in terms of uniaxial compression and tension results, without recourse to multiaxial stress versus strain curves for the benefit of engineering applications. The predicted yield surface of MFSSs from the constitutive model matches excellently with the numerical results obtained from the random beam model.

Acknowledgments

The authors are grateful for the financial support of this work by the National Natural Science Foundation of China (Nos. 11072127 and 10832002), the National Basic Research Program of China (No. 2011CB610300) and the PhD Program of Ministry of Education of China (20110002110069).

References

Alkhader, M., Vural, M., 2009. An energy-based anisotropic yield criterion for cellular solids and validation by biaxial FE simulations. J. Mech. Phys. Solids 57, 871–890.
Alkhader, M., Vural, M., 2010. A plasticity model for pressure-dependent anisotropic cellular solids. Int. J. Plast. 26, 1591–1605.
Ashby, M.F., Evans, A., Fleck, N.A., Gibson, L.J., Hutchinson, J.W., Wadley, H.N.G., 2000. Metal Foams: a Design Guide. Butterworth-Heinemann, London.
Attia, M.S., Meguid, S.A., Tan, K.T., Yeo, S.C., 2010. Influence of cellular imperfections on mechanical response of metallic foams. Int. J. Crashworthiness 15, 357–367.
Banhart, J., 2001. Manufacture, characterisation and application of cellular metals and metal foams. Prog. Mater Sci. 46. 559-553.
Bao, G., Hutchinson, J.W., McMeeking, R.M., 1991. Particle reinforcement of ductile matrices against plastic flow and creep. Acta Metall. Mater. 39, 1871–1882.
Böhm, H.J., Rammerstorfer, F.G., Weissenbek, E., 1993. Some simple models for micromechanical investigations of fiber arrangement effects in MMCs. Comput. Mater. Sci. 1, 177–194.
Chen, C., Lu, T., 2000. A phenomenological framework of constitutive modelling for incompressible and compressible elasto-plastic solids. Int. J. Solids Struct. 37, 7769–7786.
Chen, C., Lu, T.J., Fleck, N.A., 1999. Effect of imperfections on the yielding of two-dimensional foams. J. Mech. Phys. Solids 47, 2235–2272.
Christman, T., Needleman, A., Suresh, S., 1989. An experimental and numerical study of deformation in metal cerammic composites. Acta Metall. 37, 3029–3050.
Clyne, T.W., Markaki, A.E., Tan, J.C., 2005. Mechanical and magnetic properties of metal fibre networks, with and without a polymeric matrix. Compos. Sci. Technol. 65, 2492–2499.
Deshpande, V.S., Ashby, M.F., Fleck, N.A., 2001. Foam topology: bending versus stretching dominated architectures. Acta Mater. 49, 1035–1040.
Deshpande, V.S., Fleck, N.A., 2000. Isotropic constitutive models for metallic foams. J. Mech. Phys. Solids 48, 1253–1283.

Deshpande, V.S., Fleck, N.A., 2001. Multi-axial yield behaviour of polymer foams. Acta Mater. 49, 1859–1866.
Drucker, D.C., Prager, W., 1952. Soil mechanics and plastic analysis or limit design. Q. Appl. Math. 10, 157–165.
Gan, Y.X., Chen, C., Shen, Y.P., 2005. Three-dimensional modeling of the mechanical property of linearly elastic open cell foams. Int. J. Solids Struct. 42, 6628–6642.
Ghosh, S., Moorthy, S., 1995. Elastic-plastic analysis of arbitrary heterogeneous materials with the Voronoi cell finite element method. Comput. Meth. Appl. Mech. Eng. 121, 373–409.
Gibson, L.J., Ashby, M.F., 1997. Cellular Solids: Structure and Properties. Cambridge University Press.
Grenestedt, J.L., 1998. Influence of wavy imperfections in cell walls on elastic stiffness of cellular solids. J. Mech. Phys. Solids 46, 29–50.
Grenestedt, J.L., 1999. Effective elastic behavior of some models for perfect cellular solids. Int. J. Solids Struct. 36, 1471–1502.
Grenestedt, J.L., Bassinet, F., 2000. Influence of cell wall thickness variations on elastic stiffness of closed-cell cellular solids. Int. J. Solids Struct. 42, 1327–1338.
Hashin, Z., Shtrikman, S., 1963. A variational approach to the theory of the elastic behaviour of multiphase materials. J. Mech. Phys. Solids 11, 127–140.
Hill, R., 1963. Elastic properties of reinforced solids—some theoretical principles. J. Mech. Phys. Solids 11, 357–372.
Hill, R., 1965. A self-consistent mechanics of composite materials. J. Mech. Phys. Solids 13, 213–222.
Huet, C., 1990. Application of variational concepts to size effects in elastic heterogeneous bodies. J. Mech. Phys. Solids 38, 813–841.
Jiang, M., Alzebdeh, K., Jasiuk, I., Ostoja-Starzewski, M., 2001. Scale and boundary conditions effects in elastic properties of random composites. Acta Mech. 148, 63–78.
Koiter, W.T., 1960. General theorems of elastic-plastic solids. Prog. Solid Mech., 165.
Liu, J.G., Sun, G.Q., Zhao, F.L., Wang, G.X., Zhao, G., Chen, L.K., Yi, B.L., Xin, Q., 2004. Study of sintered stainless steel fiber felt as gas diffusion backing in air-breathing DMFC. J. Power Sources 133, 175–180.
Lu, T.J., He, D.P., Chen, C.Q., Zhao, C.Y., Fang, D.N., Wang, X.L., 2006. The multi-functionality of ultra-light porous metals and their applications. Adv. Mech. 36, 517–535.
Luxner, M.H., Pettermann, H.E. (2009). Modeling and simulation of highly porous open cell structures: elasto-plasticity and localization versus disorder and defects, in: Zhao, H., Fleck, N. A. (Eds.), Iutam Symposium on Mechanical Properties of Cellular Materials, pp. 125–134.
Luxner, M.H., Woesz, A., Stampfl, J., Fratzl, P., Pettermann, H.E., 2009. A finite element study on the effects of disorder in cellular structures. Acta Biomater. 5, 381–390.
Markaki, A.E., Clyne, T.W., 2003a. Mechanics of thin ultra-light stainless steel sandwich sheet material: Part I. Stiffness. Acta Mater. 51, 1341–1350.
Markaki, A.E., Clyne, T.W., 2003b. Mechanics of thin ultra-light stainless steel sandwich sheet material: Part II. Resistance to delamination. Acta Mater. 51, 1351–1357.
Meguid, S.A., Attia, M.S., Monfort, A., 2004. On the crush behaviour of ultralight foam-filled structures. Mater. Des. 25, 183–189.
Meguid, S.A., Cheon, S.S., El-Abbasi, N., 2002. FE modelling of deformation localization in metallic foams. Finite Elem. Anal. Des. 38, 631–643.
Michel, J.C., Moulinec, H., Suquet, P., 1999. Effective properties of composite materials with periodic microstructure: a computational approach. Comput. Meth. Appl. Mech. Eng. 172, 109–143.
Michel, J.C., Suquet, P., 1992. The constitutive law of nonlinear viscous and porous materials. J. Mech. Phys. Solids 40, 783–812.
Miller, R.E., 2000. A continuum plasticity model for the constitutive and indentation behaviour of foamed metals. Int. J. Mech. Sci. 42, 729–754.
Moulinec, H., Suquet, P., 1998. A numerical method for computing the overall response of nonlinear composites with complex microstructure. Comput. Meth. Appl. Mech. Eng. 157, 69–94.
Nakamura, T., Suresh, S., 1993. Effects of thermal residual stresses and fiber packing on deformation of metal-matrix composites. Acta Metall. Mater. 41, 1665–1681.
Qiao, J., Xi, Z., Tang, H., Wang, J., Zhu, J., 2009. Influence of porosity on quasi-static compressive properties of porous metal media fabricated by stainless steel fibers. Mater. Des. 30, 2737–2740.
Qiao, J.C., Xi, Z.P., Tang, H.P., Wang, J.Y., Zhu, J.L., 2008. Compressive property and energy absorption of porous sintered fiber metals. Mater. Trans. 49, 2919–2921.
Rice, J.A., 2007. Mathematical Statistics and Data Analysis. Duxbury Press.
Roberts, A.P., Garboczi, E.J., 2002a. Computation of the linear elastic properties of random porous materials with a wide variety of microstructure. Proc. R. Soc. London, Ser. A 458, 1033–1054.
Roberts, A.P., Garboczi, E.J., 2002b. Elastic properties of model random three-dimensional open-cell solids. J. Mech. Phys. Solids 50, 33–55.
Segerstad, P.H., Larsson, R., Toll, S., 2008. A constitutive equation for open-cell cellular solids, including viscoplasticity, damage and deformation induced anisotropy. Int. J. Plast. 24, 896–914.
Silva, M.J., Gibson, L.J., 1997. The effects of non-periodic microstructure and defects on the compressive strength of two-dimensional cellular solids. Int. J. Mech. Sci. 39, 549–563.
Symons, D.D., Fleck, N.A., 2008. The imperfection sensitivity of isotropic two-dimensional elastic lattices. J. Appl. Mech. 75, 051011.
Tsuda, M., Takemura, E., Asada, T., Ohno, N., Igari, T., 2010. Homogenized elastic-viscoplastic behavior of plate-fin structures at high temperatures: numerical analysis and macroscopic constitutive modeling. Int. J. Mech. Sci. 52, 648–656.
Wang, D.A., Pan, J., 2006. A non-quadratic yield function for polymeric foams. Int. J. Plast. 22, 434–458.
Wang, T.Q., 2003. Filtrating caracteristics and application of metallic fibre sintered felt. Filter & Separator 1.
Wicklein, M., Thoma, K., 2005. Numerical investigations of the elastic and plastic behaviour of an open-cell aluminium foam. Mater. Sci. Eng., A 397, 391–399.
Xi, Z., Zhu, J., Tang, H., Ao, Q., Zhi, H., Wang, J., Li, C., 2011. Progress of application researches of porous fiber metals. Materials 4, 816–824.
Zhang, J., Lin, Z., Wong, A., Kikuchi, N., Li, V.C., Yee, A.F., Nusholtz, G.S., 1997. Constitutive modeling and material characterization of polymeric foams. J. Eng. Mater. Technol. 119, 284.
Zhao, T.F. (2011). Ph. D Thesis. School of Aerospace, Xi'an Jiaotong University.
Zhou, D., Stronge, W.J., 2005. Mechanical properties of fibrous core sandwich panels. Int. J. Mech. Sci. 47, 775–798.
Zhu, H.X., Hobdell, J.R., Windle, A.H., 2000. Effects of cell irregularity on the elastic properties of open-cell foams. Acta Mater. 48, 4893–4900.